Eurofleets+

An alliance of European marine research infrastructure to meet the evolving needs of the research and industrial communities

This project has received funding from the European Union's Horizon 2020 research and innovation programme under grant agreement Nº 824077

CRUISE REPORT

Support of marine hydrate volume estimates by converted shear wave

HYDEE OBS

R/V TANGAROA, CRUISE NO. TAN2304,

21.03.2023 – 31.03.2023, WELLINGTON (NEW ZEALAND) – WELINGTON (NEW ZEALAND)

Joerg Bialas, Gareth Crutchley

Table of Content

1 Summary

On 21st March 2023 nine scientists from GEOMAR, Germany, TAMUCC, USA and GNS, New Zealand boarded R/V TANGAROA in the port of Wellington, New Zealand to prepare for EurofleetsPlus cruise TAN2304 HYDEE OBS. During two days of mobilisation 20 four component ocean-bottom seismometers (OBS), a 300 m long high-resolution seismic streamer and a 150 cinch GI airgun sent from GEOMAR, Germany, were setup for operations. In addition, NIWA, New Zealand, provided a 20” compressor container. Besides the OBS all equipment was scheduled to serve for the following cruise TAN2305 as well in order to reduce logistic costs.
In the afternoon of the 23rd March R/V TANGAROA arrived in the working area Honey Comb Ridge (Fig. 1). Here data from previous cruises revealed an anomalous seismic event with a strong inverted amplitude, reaching from the depth of a bottom simulating reflector half way into the hydrate stability zone above. Aim of the seismic investigations during HYDEE OBS is to observe converted shear waves across these structure by the deployment of OBS. Adding information on lateral and depth distribution of shear modulus in sediments will enable to test for a possible co-existence of gas and hydrate. Further these data will help to investigate the mechanism of gas migration into the hydrate stability zone and the related formation of concentrated hydrate deposits. To achieve these goals the OBS deployment need to be tailored for the analyses of the reduced sound velocity of shear waves. Therefore, the OBS should be deployed at a distance of 100 m only and should not deviate from the desired line of profile. With the standard free falling deployment procedure for OBS a usual drift of the instruments of some tens of meters is to be expected. Hence, deployment of the OBS was done with the deep-sea cable of R/V TANGAROA. Each OBS was lowered to about 30 m above seafloor, while the position at depth was monitored with the HIPAP USBL system of the vessel. Dynamic positioning enabled to deploy the instruments within +/- 5 m of the desired location.
A 150 cinch GI airgun provided seismic source signals up to 300 Hz. First R/V TANGAROA drifted at 1.5 kn across the deployed OBS to allow for the most dense shot spacing possible. Next the 300 m streamer was deployed and three additional airgun lines were shot. One across the line of OBS and two additional at 500 m distance left and right of the line of OBS. Records of the latter two lines will be used for orientation of the horizontal OBS sensors and definition of radial and transversal shear wave energy.
With respect to a very bad weather forecast the OBS were recovered after these lines. All data were copied and stored on mobile disks. Further streamer data were recorded afterwards to provide high-resolution, high-frequency data in the working area in addition to low frequency profiles previously acquired. The data sets will provide different resolution and frequency dependent images of the hydrate related structures. Decreasing weather conditions required to recover all gear in the afternoon of 28th March. Further forecasts of up to 11 Bft wind speed did not provide any hope to continue seismic profiling in the remaining time window of TAN2304 and it was decided to return to the port of Wellington two days earlier than scheduled.

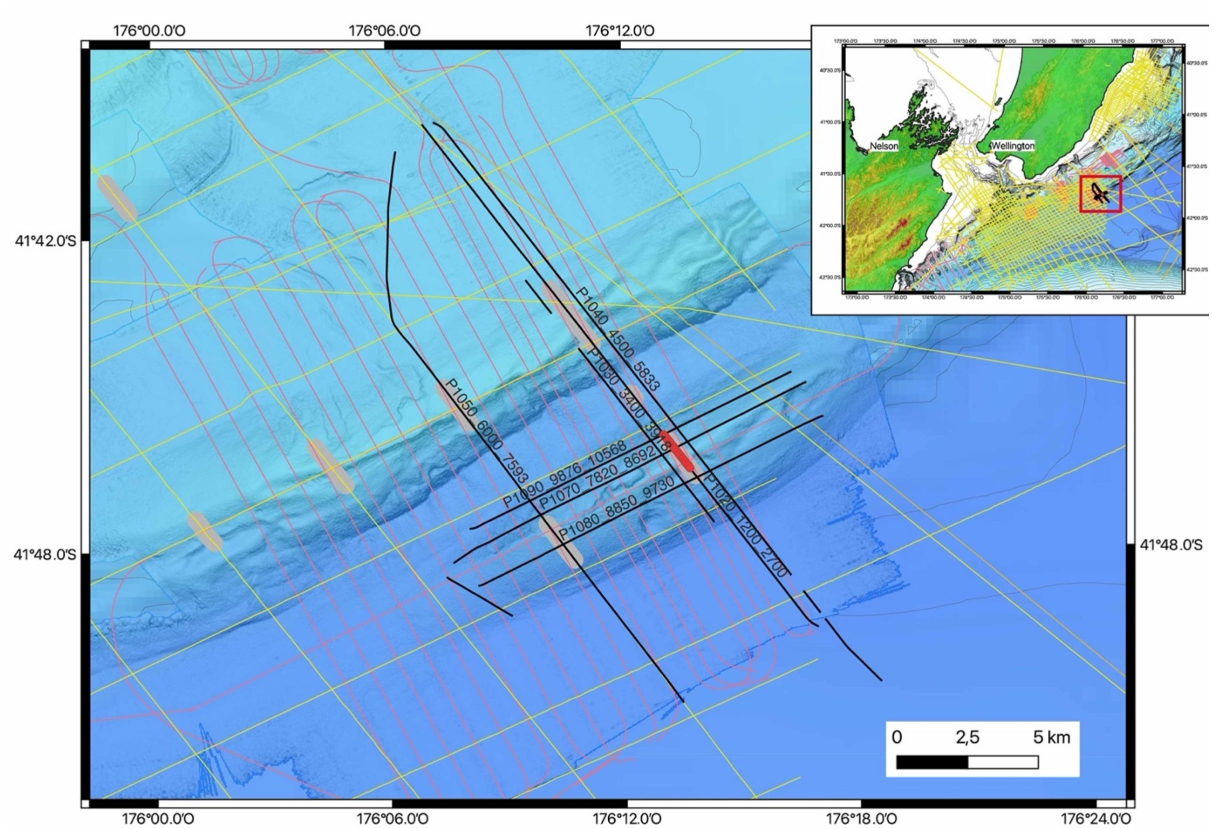

Figure 1: *Map of the OBS deployment and multichannel seismic profiling completed during cruise TAN2304 Red dots indicate OBS locations, black lines indicate TAN2304 airgun profiles, grey, red and yellow lines indicate previous MCS lines, grey areas indicate occurrence of BSR.*

2 Research Programme/Objectives

Marine gas hydrates have received much attention in recent decades (Collett et al., 2014). Gas hydrates consist of gas molecules stored in a rigid water-lattice, stable under high pressure and low temperature conditions (Sloan and Koh, 2007). There have been numerous attempts to quantify the global gas hydrate inventory (e.g. Kvenvolden and Lorenson, 2013; Milkov, 2004; Piñero et al., 2013; Wallmann et al., 2012), which is crucial for understanding the role of gas hydrates in Earth's carbon cycle. The gas hydrate system ultimately regulates how methane flows from buried marine sediments, through the seafloor, and into the oceans. The interactions at the seafloor influence the distribution and diversity of biological communities that use methane as their lifeblood (e.g. Bowden et al., 2013). The seepage of methane into the water column further influences the biogeochemistry of the oceans, with important implications for ocean acidification (e.g. Biastoch et al., 2011). In seismic measurements, a seafloor (bottom) simulating reflection (BSR) of reversed polarity compared with the seafloor, caused by free gas beneath hydrate, is the first order identifier of the base of gas hydrate stability (BGHS) (e.g. Minshull et al., 2020; Moridis et al., 2011). However, gas hydrates may be present in the absence of a BSR (Andreassen et al., 1997). Seismic wide-angle measurements provide information on hydrate distribution and concentration from velocity anomalies (Crutchley et al., 2016). Similarly, controlled source electromagnetic (CSEM) methods, sensitive to the resistivity of sediments (Hölz et al., 2015), provide additional information on sediment pore fill, which can be interpreted for gas and hydrate distribution and concentration (Schwalenberg et al., 2017).

Despite the advances made in recent decades in terms of characterizing and quantifying gas hydrate distribution (e.g. Bogoyavlensky et al., 2018; Kvenvolden and Lorenson, 2013; Piñero et al., 2013; Wallmann et al., 2012), there remains much uncertainty about gas hydrate concentration over large basin scales and at individual gas hydrate reservoirs. There is often a significant discrepancy between the concentration of gas hydrate predicted using seismic methods (i.e. using compressional and shear wave velocities) and concentrations predicted from controlled-source electromagnetic methods (i.e. using resistivity and Archie's Law)(Berndt et al.). An example of where the two methods for estimating hydrate concentrations could diverge majorly is if there is significant free gas occurring in close proximity to the gas hydrate deposits. For P-wave velocities, the occurrence of free gas will drastically reduce the velocities of the sediments, even at low concentrations (Domenico, 2012). For CSEM measurements, on the other hand, both free gas and gas hydrate will add to the bulk resistivity of the pore space (e.g. Attias et al., 2016). As such, if the occurrence of free gas together with gas hydrate cannot be isolated, there will continue to be major discrepancies between estimations of gas hydrate concentration derived from these two methods. Knowledge of additional parameters is required to provide further physical properties of the gas hydrate stability zone.

Converted shear wave (Vs) information from four component OBS measurements are sensitive to the shear modulus and can therefore help to distinguish between pore filling or cementing types of hydrate formation (Dannowski et al., 2017; Sava and Hardage, 2009). Based on this knowledge, corresponding lab experiments or rock physics models can be used to derive hydrate saturation estimates. In addition, converted shear waves can provide a much better resolution of sub-bottom strata than Vp images (Hardage et al., 2009).

Crutchley et al. (2018) investigated the large-scale distribution of concentrated gas hydrates along the accretionary Hikurangi margin. They interpreted that a pronounced asymmetry caused by preferential sedimentation on the landward sides of ridges and erosion on the seaward sides has implications for the gas hydrate system. The sedimentation on the landward side results in seafloor uplift and uplift of the base of gas hydrate stability (BGHS), which results in "gas hydrate recycling" – the liberation of free gas from gas hydrates that can then migrate back into the hydrate stability zone to re-form as gas hydrates (Fig. 2). Paull et al. (1993) suggested that such recycling of hydrate leads to the generation of higher saturation gas hydrate deposits. In contrast, erosion on the seaward sides of ridges suppresses the BGHS and is not likely to lead to hydrate recycling and concentrated gas hydrate deposits (Fig. 2). As a result, hydrate distribution across an accretionary margin might often be unbalanced as a result of these relationships between sedimentation and erosion (Crutchley et al., 2018, Fig. 2).

Seismic imaging of the differences in hydrate formation depends on the amount of hydrate formed but also on the seismic frequency available with the data acquisition (Petersen et al., 2010; Riedel et al., 2009). The low frequency content of available data makes it difficult to understand the onset and extent of hydrate formation and gas injection as the seismic events are altered by "tuning" effects caused by thin sediment layers. Tuning effects influence both the reflection strength and the phase of reflections, which makes it difficult to test the proposed model by Crutchley et al. (2018) regarding an uneven distribution and concentration of hydrates. Again, converted shear waves of four component OBS can help to investigate whether higher hydrate concentration in landward dipping sediment layers are coincident with cementation, which may not be the case on the seaward sides of ridges.

Confirmation of the above described scenario will have important implications for our understanding of global gas hydrate budgets. Moreover, it will have consequences for more localized investigations into gas hydrate production. Future gas production from hydrates will likely depend on depressurization (e.g. Moridis et al., 2011) and needs to ensure that methane cannot escape towards the seafloor (Wallmann and Bialas, 2009). Data examples from the hydrate reservoirs investigated by Crutchley et al. (2018) do show seismic reflections caused by free gas within the hydrate stability zone, well above the hydrate body. As the above described model is assumed to be applicable to accretionary margins worldwide (Crutchley et al., 2018) it is essential to understand how gas injection into the hydrate stability zone works.

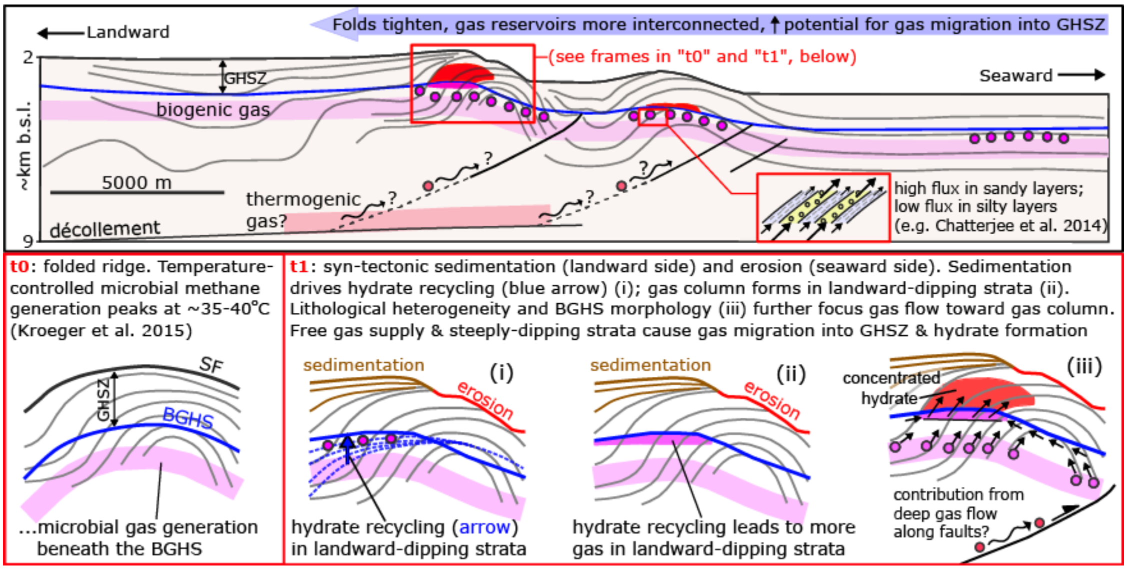

***Figure 2**: Conceptual concept on gas hydrate distribution within the slope of active margins after Crutchley et al. (2018). On the landward side of the ridge continuous sedimentation causes uplift of the BGHS, while downslope erosion causes deepening of the BGHS. With the uplift of the BGHS, long-range gas migration could preferentially occur and result in thicker, more concentrated hydrate formation than on the seaward sides of ridges.*

The overarching motivation of this project is to move towards much improved estimations of gas and gas hydrate distribution and concentration in a typical active subduction margin. As mentioned above, estimates of the global gas hydrate reservoir vary widely (Bogoyavlensky et al., 2018; Kvenvolden and Lorenson, 2013; Piñero et al., 2013; Wallmann et al., 2012), as do geophysics-based estimations of hydrate saturation at local-scale gas hydrate reservoirs (Berndt et al., 2019; Dannowski et al., 2017).

Our first aim is to test the hypothesis (Hypothesis 1) that: The co-existence of gas and gas hydrate within gas hydrate accumulations is the reason for the discrepancy in predicting hydrate saturation from seismic-based and CSEM-based methods. We will test this hypothesis through a thorough analysis of Vp, Vs and resistivity, making use of existing P-wave data (long-offset streamer seismic data APB13) (Turco et al., 2020) and S-wave velocities that we collected during this cruise. We acquired the converted S-wave data using a high-frequency source (150 cu-in GI airgun), short shot intervals (~10 m) and closely spaced OBS nodes (100 m spacing). Such a closely-spaced OBS setup is unique, and will provide excellent lateral and vertical resolution of velocities within these gas hydrate systems.

Our second aim is to determine the dominant mechanism(s) driving concentrated gas hydrate formation within an accretionary wedge setting. We will investigate the hypothesis (Hypothesis 2) that concentrated deposits are formed by free gas being injected into the gas hydrate stability zone (GHSZ) by "long-range" gas migration rather than by "short-range" methane migration (Malinverno and Goldberg, 2015). Existing seismic reflection data show indications of gas injection (Turco et al., 2020), but seismic resolution limitations in those data make it unclear how free gas is distributed and whether "tuning effects" partially cause the seismic reflectivity observed. Tuning effects in these existing data (with a dominant frequency of ∼40 Hz) make it difficult to distinguish free gas effects from interference effects caused by imaging thin layers with a low frequency source.

In order to overcome this imaging and interpretation problem we acquired an additional data set with a high-frequency source, to detect and characterize free gas migration into the GHSZ in regions where concentrated hydrates have formed. The streamer data (MCS) have a frequency range of 50-300 Hz and close receiver spacing, resulting in 1.5 m lateral resolution and ∼2-3 m vertical resolution, which greatly improves our ability to resolve free gas and gas hydrate distribution within these systems. Four component OBS were deployed above a hydrate deposit interpreted at Honey Comb ridge with indications for free gas injection into the GHSZ (Turco et al., 2020). Recording the same high frequency source signals will allow us to correlate the high resolution MCS events with OBS events and then more precisely detect free gas and hydrate reflection events in the OBS data. This will provide a more detailed velocity-depth distribution in both Vp and Vs. Comparison of these Vp and Vs models will help us to discriminate between free gas and hydrate reflection events. In the case that more-highly saturated gas hydrate formation exists within the landward dipping strata, it might be possible that massive hydrate formation has led to cementing of the host sediment. Vs reflection events will help to determine whether the type of hydrate formation (cementing or pore filling) is different on the landward and seaward sides of thrust ridges.

Our Co-PIs Constable and Kannberg (Scripps Institution of Oceanography, La Jolla) acquired CSEM data during a research cruise with R/V TANGAROA in June 2020, which enables us to draw together a diverse range of datasets. This will enable us to compare our results with resistivity-depth models. Examples from the Black Sea (Minshull et al., 2020) imaged a complex structure of increased amplitudes, partly with inverted reflection seismic events, which might be caused either by lithology changes in a complex channel-levee system or by small amounts of free gas in the HSZ. Comparing CSEM and seismic predictions of hydrate distribution and saturation has shown differences in both saturation and distribution (Minshull et al., 2020). Available seismic data off New Zealand show a clearer delineation of gas and hydrate related reflection events in a less complicated sedimentary environment. Hence, the analyses of discrepancies between CSEM and our seismic models at these deposits off New Zealand will be less influenced by complex geology.

3 Narrative of the Cruise

Cruise TAN2304 started on 21st March 2023 in the port of Wellington (Aotea Wharf) when nine scientists from three institutes (GEOMAR, GNS, TAMUCC) boarded the vessel. All new arrivals were introduced to the vessel, safety measures during work and life at sea and Corona measures (masks, daily RAT tests). NIWA loaded their 20' compressor container providing the compressed air for the GI airgun source. Seismic equipment was shipped from previous cruises off Canada and Costa Rica waiting in containers at NIWA and GNS storage sites. Urgent shipping of equipment and spares arrived from a previous cruise in the Atlantic and from GEOMAR. Helping hands at NIWA and GNS sites prepared truck loads to get all equipment alongside of R/V TANGAROA during 21st and 22nd March.

On 23rd March R/V TANGAROA left the port of Wellington at 10:30 am heading for Honey Comb ridge off Wairarapa (Fig. 1). Setup of instrumentation continued during the transit. At 17:30 hrs R/V TANGAROA arrived at the acoustic release test site. A grating box was lowered to about 1000 m water depth carrying all acoustic release devices for a test of safe operation at depth. Although one unit failed a sufficient number of releases succeeded and were prepared for deployment. After another hour of transit R/V TANGAROA arrived at the first deployment position. On site USBL guided OBS deployment began, lowering the devices to about 2,100 m water depth using the deep-sea cable. Emplacement of the first OBS (Station 100) along the spread of profile P1000 was completed on 24th March at 02:41 hrs. As scheduled a total of 20 OBS were deployed until 26th March 18:00 hrs positioning the instruments at 100 m distance on the seafloor. After recovery of the deep sea cable R/V TANGAROA moved 2 km north off the occupied line of instruments where the airgun was deployed at 20:00 hrs. Then the vessel sailed at 1 kn along a 6 km long profile across the instrumented line while triggering the GI airgun every 6 seconds. After completion of this first seismic activity on 26th March at 22:45 hrs seismic profiling was continued with deployment of the 350 m long multichannel seismic streamer. Now sailing at 4 kn the shot interval was set to 7 seconds allowing 6 seconds of data recording with the 2D streamer. At 26th March on 23:50 hrs multichannel seismic data acquisition began with the first profile crossing the OBS deployment a second time with larger distances to the first and last OBS. Next a parallel line was shot at 500 m offset west of the first profile in order to serve for orientation of the three component seismometers of the OBS later. Repeated incomplete data recording of the streamer on 27th March 03:41 hrs demand for service and a stop of multichannel recording, while airgun shooting was continued to provide further data for the OBS. Streamer recording could be restarted on 04:25 hrs. However, issues of incomplete recording continued to appear in irregular intervals. As the main task of this line was to generate seismic source signals for the OBS profiling was continued until the end of line. At 06:00 hrs the streamer was recovered and airgun shooting was interrupted. Inspection of the streamer resulted in replacement of the tow cable due to a failure of one of the build-in transmission modems. At 07:30 hrs profiling could be continued along a second parallel line, now 500 m east of the main line. In the following additional profiles were added in the vicinity of the OBS deployments occupying previous multichannel seismic lines, that were shot with lower seismic frequency content, to allow for later resolution comparison and new data analyses trials.

As the weather forecast announced wind speed of up to 21 m/s and wave height up to 8 m for the following days it was decided to stop seismic profiling on 27th March 15:13 hrs and to start OBS recovery. All 20 instruments were released one by one as the dense distance of the instruments did not allow to have more than one OBS rising in the water column at a time. On 28th March at 08:00 hrs all instruments were safely stored on board again.

Next R/V TANGAROA moved into good deployment position for streamer and airgun and continued seismic profiling at 09:30 hrs. Depth readings from three birds spread along the streamer cable showed that the tail of the streamer was towed at depth greater than the foreseen 2.5 m water depth. Therefore, it was decided to increase vessel speed to 4.5 kn through water on 28th March at 11:00 hrs. With increasing wind speed wave heights increased and caused the bird closest to the vessel to turn over for a short time about three hours later. When R/V TANGAROA turned into the next profile, now heading against wind and waves pitch and roll angle of the vessel and behavior of airgun and streamer cable in the waves became too dangerous for the equipment and it was decided to recover all gear prior to major damages on 28th March at 15:45 hrs.

The weather forecast did not improve but announced even worth conditions for the remaining three days of cruise TAN2304 and a save redeployment of streamer and airgun could not be expected. Therefore, it was decided to terminate the scientific work of TAN2304 at this time. The major task of the very dense and high resolution four channel ocean-bottom seismometer survey above a structure indicating free gas migration into the gas hydrate stability zone has been achieved. R/V TANGAROA docked in the port of Wellington on 29th March 2023 at 11:00 hrs again.

TAN2304 Operations

Date	Time	Coordinates		Depth	Action
	local	Longitude [E]	Latitude [S]	[m]	
21.03.23	10:00	port of Wellington			9 scientists boarding
					safety instruction
					on board familirisation
					start preparing laboratories
					loading airgun and streamer
22.03.23	08:00	port of Wellington			general meeting
					loading of compressor
					loading of OBS
					preparation of streamer
					preparation of OBS
23.03.23	08:00	port of Wellington			prepare for departure
	10:00	leave port of Wellington			
	17:30	1000 m water depth			test of acoustic release devices at depth
24.03.23	02:40	176°13'	41°45.8'	2284	deploy OBS 100
	06:30				OBS 101 entangled in deep-sea cable
	09:18	176°13.059'	41°45.87'	2270	deploy OBS 101
					speed of cable reduced to 0.25 m/s
	12:17	176°13.104'	41°45.916'	2261	deploy OBS 102
	15:38	176°13.157'	41°45.957'	2249	deploy OBS 103
					difficulties with USBL transponder
					spare unit mounted
	21:36	176°13.190'	41°45.995'	2244	deploy OBS 104
25.03.23	00:26	176°13.241'	41°46.043'	2229	deploy OBS 105
	03:19	176°13.288'	41°46.088'	2220	deploy OBS 106
	06:27	176°13.323'	41°46.125'	2206	deploy OBS 107
	09:44	176°13.37'	41°46.165'	2195	deploy OBS 108
	12:23	176°13.412'	41°46.213'	2185	deploy OBS 109
	15:54	176°13.462'	41°46.257'	2185	deploy OBS 110
	19:11	176°13.502'	41°46.297'	2189	deploy OBS 111
	21:52	176°13.548'	41°46.34'	2211	deploy OBS 112
26.03.23	00:32	176°13.585'	41°46.383	2246	deploy OBS 113
	03:13	176°13.637'	41°46.428'	2269	deploy OBS 114
	06:21	176°13.68'	41°46.47'	2288	deploy OBS 115
	09:09	176°13.717'	41°46.510'	2292	deploy OBS 116
	11:53	176°13.757'	41°46.555'	2294	deploy OBS 117
	14:49	176°13.805'	41°46.6'	2301	deploy OBS 118
	17:36	176°13.851'	41°46.635'	2323	deploy OBS 119
	18:31	176°10.809'	41°43.658'	2382	SOL P1000
	20:42	176°15.085'	41°47.831'	2726	EOL P1000
	21:50	176°16.464'	41°49.198	2726	Streamer deployed
					SOL P1020
27.03.23	00:40	176°06.957'	41°39.898	2083	EOL P1020
	00:49	176°06.758	41°40.158'	2083	SOL P1030
	02:10	176°11.080	41°44.373'	2156	restart recording
	04:00	176°17.555'	41°50.4'		stop recording; streamer not respondning
					EOL P1030
					stop airgun; recover streamer
					replace tow cable
	05:24	176°18.565'	41°50.611'		start airgun; continue recording
	05:53	176°16.839'	41°49.123'	2726	SOL P1040
	08:47	176°07.068'	41°39.784	2084	EOL P1040
	09:12	176°06.093'	41°41.07'	2084	SOL P1045
	09:50	176°06.160'	41°43.675'	2102	EOLP1045
					SOLP1050
	13:13	176°13.563'	41°51.052'	2719	EOL P1050; recover airgun & streamer
	14:55	176°13.851'	41°46.635'	2323	recover OBS 119

	16:25	176°13.805'	41°46.6'	2301	recover OBS 118
	17:25	176°13.757'	41°46.555'	2294	recover OBS 117
	18:12	176°13.717'	41°46.510'	2292	recover OBS 116
	19:09	176°13.68'	41°46.47'	2288	recover OBS 115
	19:55	176°13'	41°45.8'	2284	recover OBS 100
	20:41	176°13.059'	41°45.87'	2270	recover OBS 101
	21:18	176°13.104'	41°45.916'	2261	recover OBS 102
	21:55	176°13.157'	41°45.957'	2249	recover OBS 103
	22:40	176°13.190'	41°45.995'	2244	recover OBS 104
	23:35	176°13.241'	41°46.043'	2229	recover OBS 105
28.03.23	00:00	176°13.288'	41°46.088'	2220	recover OBS 106
	00:45	176°13.323'	41°46.125'	2206	recover OBS 107
	01:32	176°13.37'	41°46.165'	2195	recover OBS 108
	02:15	176°13.412'	41°46.213'	2185	recover OBS 109
	03:35	176°13.462'	41°46.257'	2185	recover OBS 110
	04:15	176°13.502'	41°46.297'	2189	recover OBS 111
	05:04	176°13.548'	41°46.34'	2211	recover OBS 112
	06:02	176°13.585'	41°46.383	2246	recover OBS 113
	07:20	176°13.637'	41°46.428'	2269	recover OBS 114
	09:00				deploy airgun & streamer
	09:32	176°08.88'	41°49.167'	2646	SOL P1065
	10:00	176°07.996'	41°48.075'	2541	EOL P1065
					SOL P1070
	11:38	176°16.654'	41°44.855'	2261	EOL P1070
	11:59	176°17.090'	41°45.481'	2418	SOL P1080
	12:40	176°08.546'	41°48.593'	2462	EOL P1080
	13:01	176°08.258'	41°47.561'	2567	SOL P1090
	14:17	176°16.414'	41°44.61'	2267	EOL P1090
	14:36	176°16.848'	41°45.126'	2346	SOL P1100
	14:45	176°16.015'	41°45.437'	2263	EOL P1100
					recover airgun & streamer
					stop surveying due to bad weather conditions
	16:00				weather forecast up to Bft 11 the next days
					weather forecast to bad to resume survey
29.03.23	11:00	port of Wellington			end of TAN2304 survey

Table 1: Operations, deployments and recoveries during cruise TAN2304.

4 Preliminary Results

20 ocean-bottom seismometers (OBS), a 350 m long multichannel seismic streamer and a GI airgun (150 cinch) were provided by GEOMAR for high resolution investigations of converted shear waves at Honey Comb ridge.

4.1 System Overview

4.1.1 Ocean-Bottom Seismometers

GEOMAR ocean-bottom seismometers (OBS) are autonomous platforms carrying a hydrophone and a three-component seismometer (Fig. 3). Analogue data from the two sensors are digitized by a custom build GEOLOG recording device. The temperature controlled internal clock of the GEOLOG is synchronized with a GPS receiver prior to deployment. Data storage is done on two micro-SD cards. The data logger is stored with alkaline batteries in a titanium pressure tube. During standard deployment procedures the OBS is released at the sea surface on the desired deployment location and descends to the seafloor through negative buoyancy caused by an iron anchor weight. The low descending speed of about 0.4 m/s allows lateral deviation from the desired deployment position due to water currents. Although such deviations usually are within a few tens of meters the aim for high resolution records of converted shear wave events demand for a better control and more precise deployment. Hence it was decided to lower the OBS by the deep sea cable of R/V TANGAROA to about

20 m above seafloor. Therefore, a heavy duty release was attached to the deep sea cable together with a HIPAP USBL pinger. Then the recovery rope of the OBS was hooked into the heavy duty release. On site the OBS was lowered to the sea surface by a crane, while the deep sea cable and the heavy duty release were swung out by the A-frame. Once released the OBS descend until the recovery rope and the deep sea cable took its load and payout of cable began. Payout speed need to be lower than the descent rate and was chosen to 0.4 m/s. Supported by HIPAP USBL navigation it was possible to navigate the wet end of the deep sea cable within +/- 5 m offset to the desired deployment position. Then a heavy duty release was used to release the OBS and let it descend the remaining 20 m to the seafloor (Fig. 4).

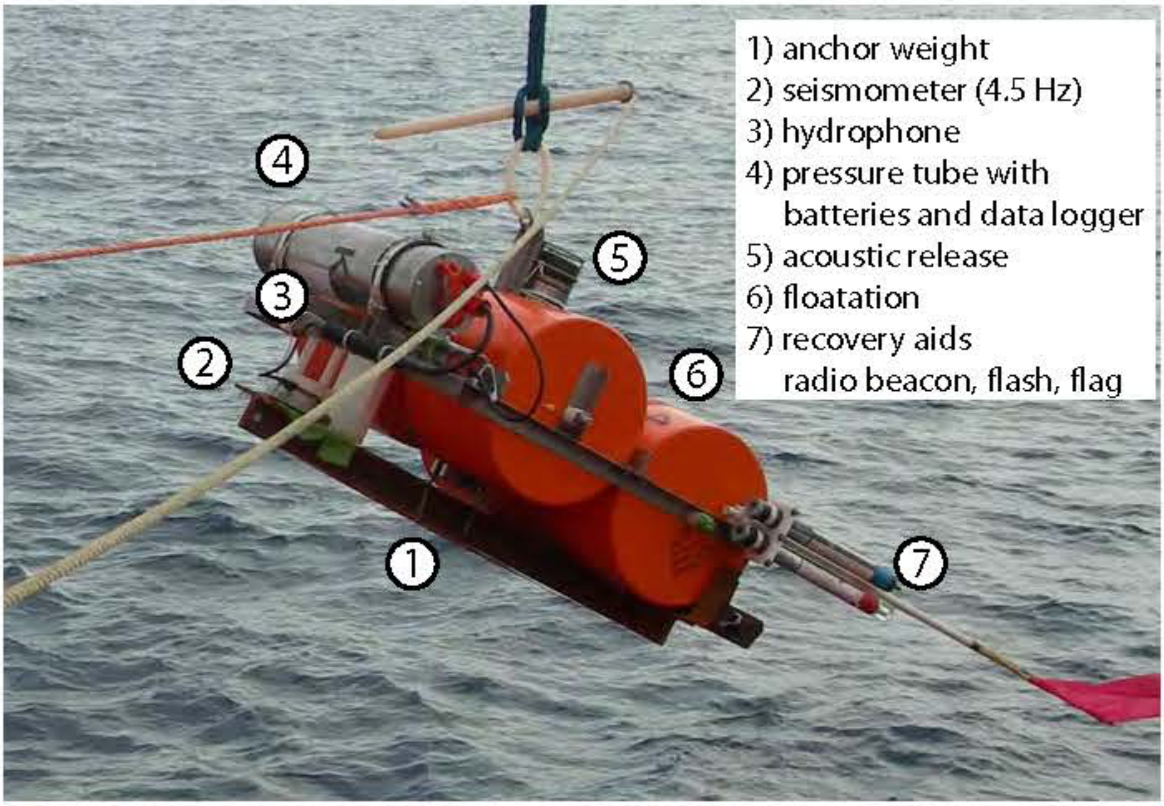

Figure 3: A GEOMAR OBS during standard free fall deployment

Following this procedure all 20 OBS were deployed with a time effort of about 3 hrs per station. However, without this time consuming process it would not be possible to ensure a regular deployment scheme of 100 m distance between the instruments and a good alignment of all instruments along the desired profile line. Nevertheless, there is no control of orientation of the OBS and the attached seismometer. As the seismometer is not equipped with a compass device the orientation of the horizontal sensors is not known. Therefore, two additional airgun profiles were shot left and right of the main line at about 500 m offset. The resulting angular airgun source signals will allow us to analyses the time (azimuth) of maximum energy for the horizontal components and provide the information to virtually rotate the sensors in an inline and crossline orientation during post-processing.

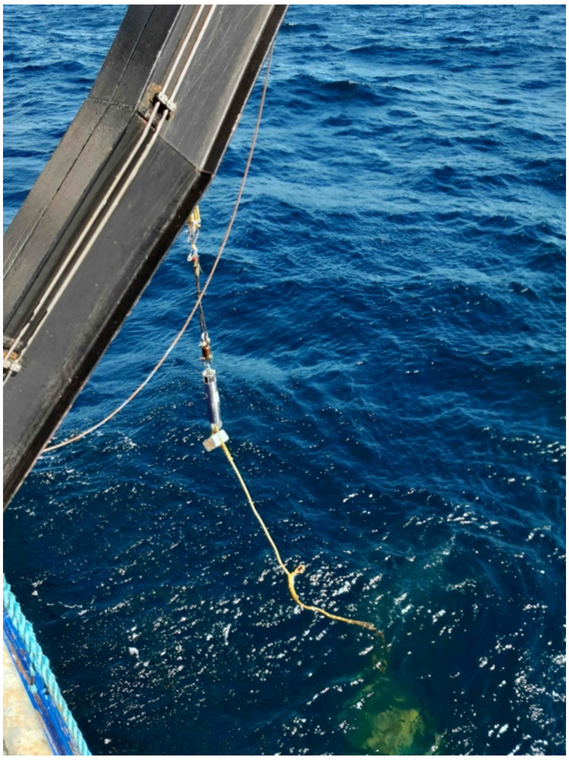

Figure 4: Photographs of the cable controlled deployment on board R/V TANGAROA
Left: The OBS is lowered to the sea surface while the deep sea cable with HIPAP USBL Pinger and heavy duty release are ready for payout of cable.
Right: The OBS already descending while the recovery rope is attached to the heavy duty release. This configuration is then lowered down to about 20 m above seafloor. Release of the heavy duty release lets the OBS descend the final meters into position at the seafloor.

4.1.2 Multichannel Streamer

During cruise TAN2304 HYDEE OBS a high-resolution digital multichannel streamer was provided by GEOMAR. The streamer was operated from a winch that was welded to the working deck of R/V TANGAROA (Fig. 5). The winch was connected via a deck cable with the control and recording device in the dry lab. The streamer comprises a 100 m long tow cable, a 20 m long stretch section and 19 active sections of 12.5 m length. Each active section of the streamer holds 8 channels at 1.5625 m distance. Depth control of the streamer was provided through three active birds, one attached on the stretch section, one attached to a 1.5625 m bird section between active section 11 & 12 (causing one dead trace count) and a third behind active section 19 (Fig. 8). Target depth of the birds was set to 4.5 m.

Two streamer deployments were undertaken during the survey. During the first deployment the tow cable was paid out for a length of 40 m behind the stern of the vessel. It turned out that towing angle and the frontal section caused too much tension on the cable, avoiding successful depth regulation by the first bird. The resulting towing depth was shallower than 4 m for the first active channels. Towards the end weight of the solid-state streamer sections could not be fully compensated by the third bird and the last active channels were towed at a depth deeper than 4 m. After a failure of the towing cable and replacement it was paid out for 53 m. However, towing forces did not allow the first bird to regulate the depth of the first active channels at the desired 4 m depth.

Figure 5: Streamer winch with the multichannel streamer on the drum. In the background two depth controller (birds) are prepared for attachment once the streamer is deployed.

4.1.3 Airgun Source

In order to serve for the desired high resolution of the seismic events in the hydrate stability zone and to comply with the environmental obligations to protect marine mammals a GI airgun with a total volume of 150 cinch was chosen as seismic source (Fig. 6). The gun floatation was provided with a new prototype of a GPS receiver box to monitor the track of the gun and to avoid deviations in gun position during layback calculations based on ships heading, course and length of the gun tow cable. The airgun was prepared at the bridge above the working deck at the aft of the vessel. Towing point for the umbilical was at the portside of the vessel. Length of the towing cable was 22 m behind the aft of the vessel. The gun was towed at 2 m water depth.

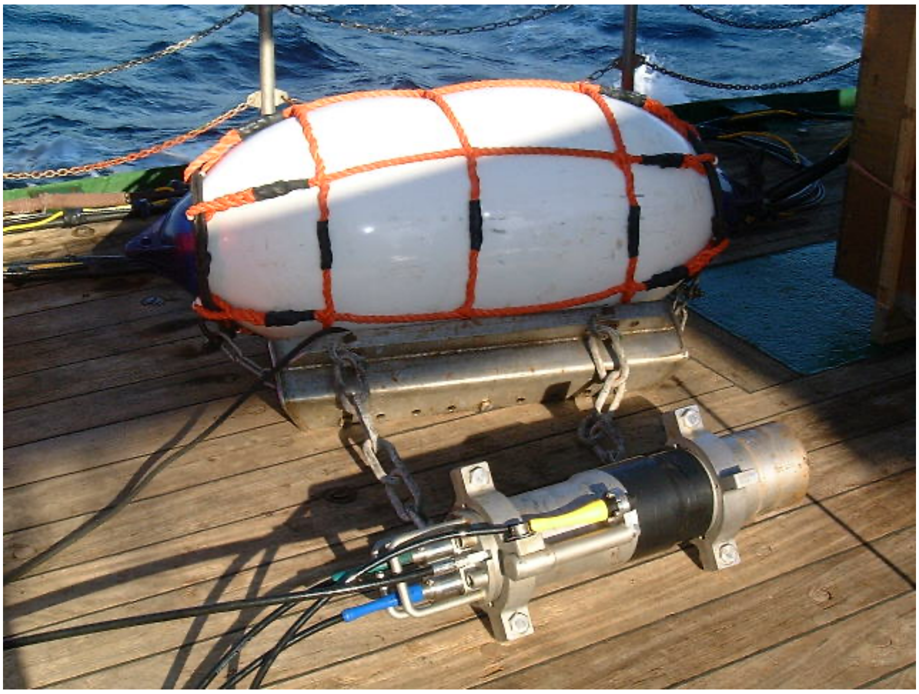

Figure 6: Photograph of the 150 cinch GI airgun and the floatation

Compressed air for the airgun operation was provided by NIWA's Price compressor (Fig. 7). The compressor provided 150 bar working pressure continuously throughout the survey.

Figure 7: NIWA's Price compressor container onboard R/V TANGAROA

4.1.4 Cable Setting on Board

Seismic source signal generation by the GI airgun was based on an automatic trigger synchronized by GPS time signal in the dry lab. The trigger signal was delivered to the airgun controller device (LongShot) and the streamer control and recording unit (GPSU). The LongShot was set to ignite the airgun with a delay of 50 ms (aim point). The signal of an airgun pulse detection hydrophone was analyzed and used to constantly calibrate a regular shot interval. With each trigger signal the ships position was recorded from the GPS antenna setup for the trigger timing device (Fig. 8). Relative measures of the gun, streamer and respective tow cables to the antenna position are given in Figure 8.

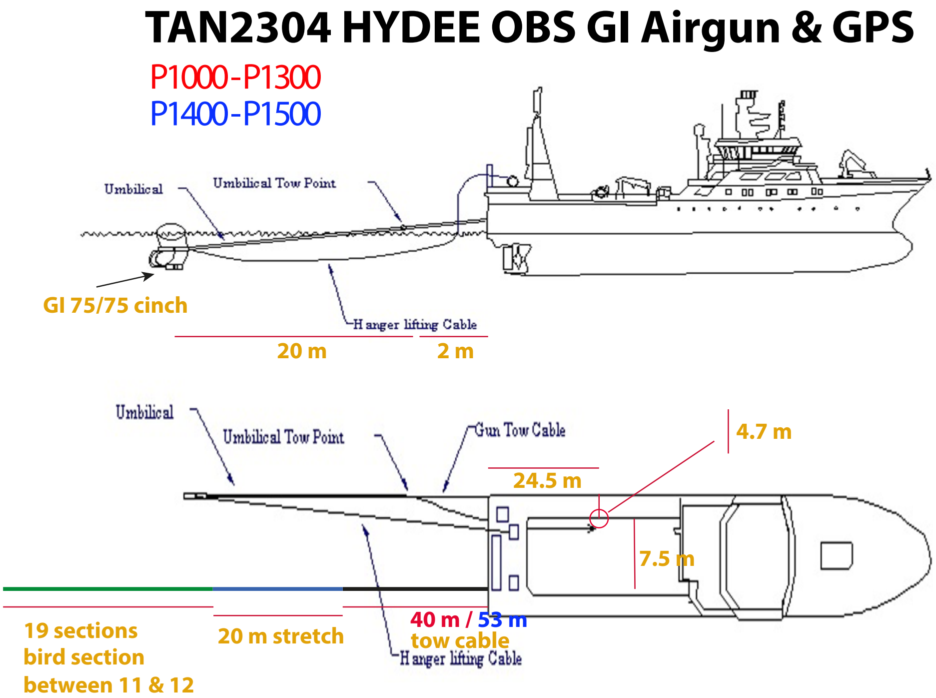

Figure 8: Map of GPS antenna position and relative distances for airgun, streamer and tow cables

4.2 Work Completed

Field work of cruise TAN2304 began with cable controlled deployment of 20 Ocean-Bottom seismometers (OBS) across the Honey Comb ridge (Fig. 1). During this process the ship's HIPAP USBL system and a mobile transponder at the wet end of the deep-sea cable was used to maneuver the OBS as close as +/- 5 m to its desired deployment position. Thereby, the instruments could be setup at 100 m distance to each other without any drift offset for the desired seismic shooting line.

Next R/V TANGAROA sailed to a position 1.5 nm north of the line of OBS and deployed the GI airgun. In order to achieve the shortest distance between consecutive shots the vessel drifted with 1 kn to 1.5 kn along the line of OBS firing the airgun every 7 secs (Survey P1000).

For the following surveys the high-resolution multichannel streamer (MCS) was deployed. Profiling started at about 4 nm distance to the southernmost OBS. First survey P1020 was shot across the OBS to serve for further offset observations of the instruments. A first onboard processing of the streamer observations (Fig. 9) confirmed a suitable penetration of the seismic energy to image the bottom simulating reflector (BSR) and the anomalous reflecting events (3.4 s to 3.7 s two-way traveltime (TWT)) above.

In the following two parallel lines (surveys P1030 to P1400) were shot each 500 m offset to the west and east of the main OBS line. Shot records of this surveys will be used to detect the azimuths of the horizontal sensors of the seismometers at the seafloor. Further processing will distribute seismic energy into radial and transversal components for the analyses of converted shear wave events.

Due to weather conditions the OBS were recovered after completion of these survey lines. Data copies were stored at the server and on mobile disks. Based on the streamer records the airgun position was determined and first navigation tables were provided to allow a preview of the OBS data.

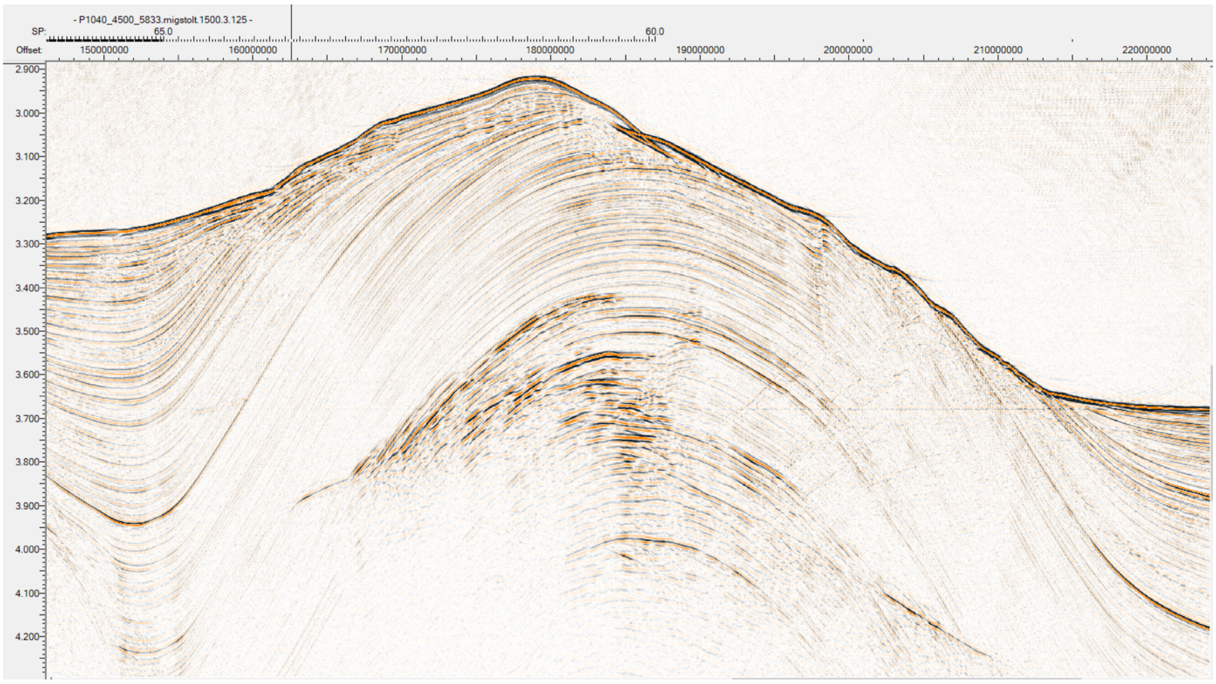

Figure 9: High resolution multichannel seismic reflection line across Honey Comb ridge. Processing included 3 Hz to 125 Hz frequency filter and a Stolt time migration using 1500 m/s water sound velocity.

First seismic sections of the OBS data show very promising results (Fig. 10 & 11). Optimized data processing (e.g., time dependent deconvolution) still need to be applied. However, a simple bandpass filter (20 Hz to 200 Hz) revealed a series of reflections following the direct water wave, which appears as the first event in the OBS sections. In the center of the OBS sections traveltimes are comparable to the MCS data (Fig. 9). Here two strong events are observed on the hydrophone and vertical component at 400 ms to 700 ms TWT (Fig. 10). The first event appears with an inverted amplitude compared to the direct wave, while the second event shows the same amplitude orientation. This might already be interpreted as a first hint for changes in physical parameters at this depth interval.

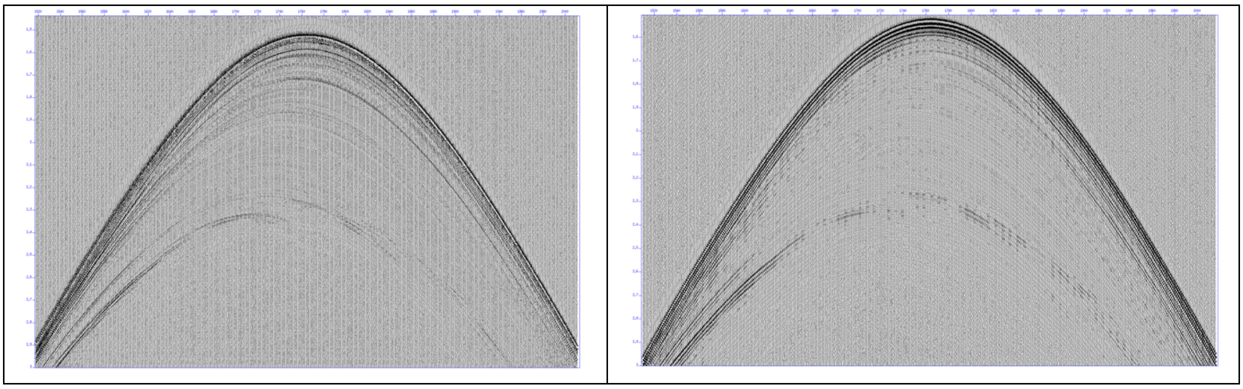

Figure 10: Seismogram of the hydrophone (left) and vertical (right) sensor of OBS 101 recording airgun shots of survey P1020. Besides a frequency filter (20 Hz to 200 Hz bandpass) no further processing was applied.

The same event is observed on the horizontal components of the OBS (Fig. 11). Obviously, a significant part of the seismic energy travelling with the compressed wavefield was coupled into the horizontal sensors. This might happen in case of a significant tilt of the seismometer. However, at later arrival times further strong reflection events are observed that do not appear on the vertical and the hydrophone section. Most probably those events represent converted shear wave energy that does travel with significant lower sound velocity after conversion from compression to shear. During the process of reorientation of the seismometer the seismic energy will be redistributed into vertical, radial and transverse contributions. Hence the strong cross coupling of compressional energy will be removed from the horizontal components and allow a more prominent display of the converted shear energy.

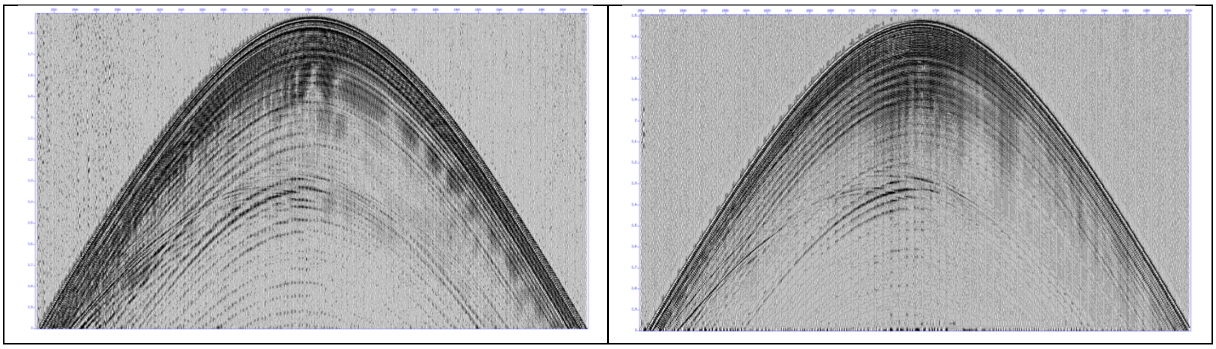

Figure 11: Seismogram of the two horizontal sensors of OBS 101 observing seismic events along survey P1020. The energy distribution has not yet been corrected for radial and transversal orientation. A bandpass filter of 20 Hz to 200 Hz has been applied.

5 Data and Sample Storage / Availability

The Kiel Data Management Team (KDMT) at GEOMAR maintains the publicly accessible Ocean Science Information System (OSIS) as a central information and research data sharing utility. OSIS merges information on expeditions, experiments, and numerical models with peer review publications and available research data. OSIS is open to the public while access to actual data in ongoing research projects may be restricted for definable periods of time. However, the status of data files and contact person is visible and may foster collaborations with interested researchers. In addition, KDMT members are active PANGAEA data curators and will assist with data publication in a World Data Center (e.g. PANGAEA) which will then warrant long-term archival and access to the research data. Cooperation with a world data center and the union for application of International Geo Sample Numbers (IGSN) will make data and samples globally trackable and increase their scientific value and usability. Free access to the data will be granted after a moratoroium of two years.

6 Participants

No.	Name	Early Career	Gender	Affiliation	On-Board Task
1	Joerg Bialas	N	M	GEOMAR	Voyage Leader
2	Gareth Crutchley	N	M	GEOMAR	Co-Voyage Leader, processing
3	Christian Berndt	N	M	GEOMAR	Multichannel seismic
4	Gero Wetzel	N	M	GEOMAR	Engineer
5	Bruna Pandolpho	Y	F	GEOMAR	Watch keeper
6	Henrike Timm	Y	F	GEOMAR	Watch keeper
7	Ingo Pecher	N	M	TAMUCC	OBS
8	Karsten Kroeger	N	M	GNS	OBS, observer
9	Jason Farr	N	M	GNS	Technician

Participants were not funded through Eurofleets+.

GEOMAR GEOMAR Helmholtz Centre for Ocean Research Kiel, Kiel, Germany

GNS Institute of Geological and Nuclear Sciences, Lower Hutt, New Zealand

TAMUCC Texas A&M University Corpus Christi, Corpus Christi, USA

7 Station List

See Table 1 in Chapter 3.

8 Acknowledgements

Survey TAN2304 has been provided through the EUROFLEETSPlus Sea program Call Oceans under Grant #824077 in 2019. Due to the worldwide restrictions in travel and work during the Corona pandemic the cruise was delayed until March 2023. Our thanks go to Eurofleets+ and ship operator NIWA having kept the Grant alive and providing ship time with such a delay. With GEOMAR as European research institute and NIWA as ship operator based in New Zealand two parties operating under completely different legal frameworks needed to agree on a contract satisfying the legal demands of both. Besides Rob Christie (NIWA) and Kirsten Hoppe (GEOMAR) we thank all involved persons who helped to reiterate the related contract forms. Our thanks also go to Regina Eisert (MBIE), Niamh Flavin and Bernadette Ni Chonghaile (both at the Eurofleets+ Coordination Office) for the distinguished assistance with aspects related to logistics and funding. Karen Keddy and the logistics team of NIWA helped a lot to get incoming and outgoing cargo shipments in good order. Will Quinn provided excellent technical support through the supply of NIWA's HiPAP ultra short baseline (USBL) system for accurate positioning of instruments on the seafloor. Captain Mark Hansen and his crew provided a more than excellent support during our operations at sea.

9 References

Andreassen, K., Hart, P. E., and MacKay, M., 1997, Amplitude versus offset modeling of the bottom simulating reflection associated with submarine gas hydrates: Marine Geology, v. 137, no. 1-2, p. 25 - 40.

Attias, E., Weitemeyer, K. A., Minshull, T. A., Best, A. I., Sinha, M., Jegen-Kulcsar, M., Hölz, S., and Berndt, C., 2016, Controlled-source electromagnetic and seismic delineation of sub-seafloor fluid flow structures in a gas hydrate province, offshore Norway: Geophysical Journal International, v. 206, no. 1093-1110, p. 1 - 35.

Berndt, C., Chi, W. C., Jegen, M., Lebas, E., Crutchley, G., Muff, S., Hölz, S., Sommer, M., Lin, S., Liu, C. S., Lin, A. T., Klaeschen, D., Klaucke, I., Chen, L., Hsu, H. H., Kunath, P., Elger, J., McIntosh, K. D., and Feseker, T., 2019, Tectonic Controls on Gas Hydrate Distribution Off SW Taiwan: Journal of Geophysical Research: Solid Earth, v. 124, no. 2, p. 1164 - 1184.

Biastoch, A., Treude, T., Rüpke, L. H., Riebesell, U., Roth, C., Burwicz, E. B., Park, W., Latif, M., Böning, C. W., Madec, G., and Wallmann, K., 2011, Rising Arctic Ocean temperatures cause gas hydrate destabilization and ocean acidification, v. 38, no. 8, p. 5.

Bogoyavlensky, V., Kishankov, A., Yanchevskaya, A., and Bogoyavlensky, I., 2018, Forecast of Gas Hydrates Distribution Zones in the Arctic Ocean and Adjacent Offshore Areas: Geosciences, v. 8, no. 12, p. 453.

Bowden, D. A., Rowden, A. A., Thurber, A. R., Baco, A. R., Levin, L. A., and Smith, C. R., 2013, Cold Seep Epifaunal Communities on the Hikurangi Margin, New Zealand: Composition, Succession, and Vulnerability to Human Activities: PLoS ONE, v. 8, no. 10, p. e76869 - 76820.

Collett, T., Bahk, J.-J., Baker, R., Boswell, R., Divins, D., Frye, M., Goldberg, D., Husebø, J., Koh, C., Malone, M., Morell, M., Myers, G., Shipp, C., and Torres, M., 2014, Methane Hydrates in Nature—Current Knowledge and Challenges: Journal of Chemical & Engineering Data, v. 60, no. 2, p. 319 - 329.

Crutchley, G. J., Kroeger, K. F., Pecher, I. A., and Gorman, A. R., 2018, How tectonic folding influences gas hydrate formation: New Zealand's Hikurangi subduction margin, v. 47, no. 1, p. 39 - 42.

Crutchley, G. J., Maslen, G., Pecher, I. A., and Mountjoy, J. J., 2016, High-resolution seismic velocity analysis as a tool for exploring gas hydrate systems: An example from New Zealand's southern Hikurangi margin: Interpretation, v. 4, no. 1, p. SA1 - SA12.

Dannowski, A., Bialas, J., Schwalenberg, K., Gehrmann, R., Zander, T., and Kläschen, D., Shear wave modelling of high resolution OBS data with a comparison to CSEM data in a gas hydrate environment in the Danube deep-sea fan, Black Sea2017, p. 1 - 2.

Domenico, S. N., 2012, EFFECT OF BRINE-GAS MIXTURE ON VELOCITY IN AN UNCONSOLIDATED SAND RESERVOIR: Geophysics, v. 41, no. 5, p. 882 - 894.

Hardage, B. A., Murray, P. E., Remington, R., Angelo, M. D., Sava, D., Roberts, H. H., Shedd, W., and Jr, J. H., 2009, Multicomponent Seismic Technology Assessment of Fluid-gas Expulsion Geology and Gas-hydrate Systems: Gulf of Mexico, *in* T Collett, A. J. C. K. R. B., ed., Volume 89, p. 247 - 265.

Hölz, S., Swidinsky, A., Sommer, M., Jegen, M., and Bialas, J., 2015, The use of rotational invariants for the interpretation of marine CSEM data with a case study from the North Alex mud volcano, West Nile Delta: Geophysical Journal International, v. 201, no. 1, p. 224 - 245.

Kvenvolden, K. A., and Lorenson, T. D., 2013, The Global Occurrence of Natural Gas Hydrate, Volume 8, American Geophysical Union, p. 3 - 18.

Malinverno, A., and Goldberg, D. S., 2015, Testing short-range migration of microbial methane as a hydrate formation mechanism: Results from Andaman Sea and Kumano Basin drill sites and global implications: Earth and Planetary Science Letters, v. 422, p. 105 - 114.

Milkov, A. V., 2004, Global estimates of hydrate-bound gas in marine sediments: how much is really out there?: Earth-Science Reviews, v. 66, no. 3–4, p. 183 - 197.

Minshull, T. A., Marín-Moreno, H., Betlem, P., Bialas, J., Bünz, S., Burwicz, E., Cameselle, A. L., Cifci, G., Giustiniani, M., Hillman, J. I. T., Hölz, S., Hopper, J. R., Ion, G., León, R., Magalhaes, V., Makovsky, Y., Mata, M.-P., Max, M. D., Nielsen, T., Okay, S., Ostrovsky, I., O'Neill, N., Pinheiro, L. M., Plaza-Faverola, A. A., Rey, D., Roy, S., Schwalenberg, K., Senger, K., Vadakkepuliyambatta, S., Vasilev, A., and Vázquez, J.-T., 2020, Hydrate occurrence in Europe: A review of available evidence: Marine and Petroleum Geology, v. 111, p. 735-764.

Moridis, G. J., Collett, T. S., Pooladi-Darvish, M., Hancock, S., Santamarina, C., Boswell, R., Kneafsey, T., Rutqvist, J., Kowalsky, M. B., Reagan, M. T., Sloan, E. D., Sum, A. K., and Koh, C. A., 2011, Challenges, Uncertainties, and Issues Facing Gas Production From Gas-Hydrate Deposits: Spe Reservoir Evaluation & Engineering, v. 14, no. 1, p. 76 - 112.

Paull, C. K., Ussler, W., III, and Borowski, W. S., 1993, Sources of biogenic methane to form marine gas hydrates: In situ production or upward migration?

Petersen, C. J., Bünz, S., Hustoft, S., Mienert, J., and Klaeschen, D., 2010, High-resolution P-Cable 3D seismic imaging of gas chimney structures in gas hydrated sediments of an Arctic sediment drift: Marine and Petroleum Geology, v. 27, no. 9, p. 1981 - 1994.

Piñero, E., Marquardt, M., Hensen, C., Haeckel, M., and Wallmann, K., 2013, Estimation of the global inventory of methane hydrates in marine sediments using transfer functions: Biogeosciences, v. 10, no. 2, p. 959 - 975.

Riedel, M., Willoughby, E. C., Edwards, N., Hyndman, R. D., Spence, G. D., Chapman, R., Chen, M.-A., Novosel, I., and Schwalenberg, K., 2009, Gas Hydrate Offshore Vancouver Island, Northern Cascadia Margin, *in* T Collett, A. J. C. K. R. B., ed., p. 433 - 450.

Sava, D., and Hardage, B., 2009, Chapter 20: Rock-physics Models for Gas-hydrate Systems Associated with Unconsolidated Marine Sediments, *in* T S Collett, A. H. J. C. K. R. B., ed., Volume 89, p. 505 - 524.

Schwalenberg, K., Hölz, S., Gehrmann, R., Rippe, D., Dannowski, A., Zander, T., Duan, S., Jegen, M., and Bialas, J., Gas hydrate occurrences in the Danube Delta, Western Black Sea: Results from 2D and 3D controlled source electromagnetics2017, Volume 19, p. 18311.

Sloan, E. D. J., and Koh, C. A., 2007, Clathrate Hydrates of Natural Gases, TAylor & Francis, 752 p.:

Turco, F., Crutchley, G. J., Gorman, A. R., Mountjoy, J. J., Hillman, J. I. T., and Woelz, S., 2020, Seismic velocity and reflectivity analysis of concentrated gas hydrate deposits on the southern Hikurangi Margin (New Zealand): Marine and Petroleum Geology, v. 120.

Wallmann, K., and Bialas, J., 2009, SUGAR (submarine gas hydrate reservoirs): Environmental Earth Sciences, v. 59, no. 2, p. 485-487.

Wallmann, K., Burwicz, E., Rüpke, L., Piñero, E., Haeckel, M., and Hensen, C., 2012, The global inventory of methane hydrate in marine sediments: A theoretical approach, v. 5, p. 2449 - 2498.